Remote Sensing of Environment 152 (2014) 364–374

Contents lists available at ScienceDirect

Remote Sensing of Environment

journal homepage: www.elsevier.com/locate/rse

Marsh Dieback, loss, and recovery mapped with satellite optical, airborne polarimetric radar, and field data

Elijah Ramsey III [a,*], Amina Rangoonwala [b], Zhaohui Chi [c], Cathleen E. Jones [d], Terri Bannister [c]

[a] U.S. Geological Survey, National Wetlands Research Center, 700 Cajundome Blvd., Lafayette, LA 70506, USA
[b] Five Rivers Services, LLC, 10807 New Allegiance Drive, Colorado Springs, CO 80918, USA
[c] University of Louisiana-Lafayette CESU, 635 Cajundome Blvd, Lafayette, LA 70506, USA
[d] Jet Propulsion Laboratory, California Institute of Technology, 4800 Oak Grove Dr., Pasadena, CA 91109, USA

ARTICLE INFO

Article history:
Received 24 October 2013
Received in revised form 10 July 2014
Accepted 12 July 2014
Available online 2 August 2014

Keywords:
Spartina alterniflora marsh dieback
Optical vegetation indexes
NASA UAVSAR
Polarimetric synthetic aperture radar (PolSAR)
Coastal wetlands

ABSTRACT

Landsat Thematic Mapper and Satellite Pour l'Observation de la Terre (SPOT) satellite based optical sensors, NASA Uninhabited Aerial Vehicle synthetic aperture radar (UAVSAR) polarimetric SAR (PolSAR), and field data captured the occurrence and the recovery of an undetected dieback that occurred between the summers of 2010, 2011, and 2012 in the *Spartina alterniflora* marshes of coastal Louisiana. Field measurements recorded the dramatic biomass decrease from 2010 to 2011 and a biomass recovery in 2012 dominated by a decrease of live biomass, and the loss of marsh as part of the dieback event. Based on an established relationship, the near-infrared/red vegetation index (VI) and site-specific measurements delineated a contiguous expanse of marsh dieback encompassing 6649.9 ha of 18,292.3 ha of *S. alterniflora* marshes within the study region. PolSAR data were transformed to variables used in biophysical mapping, and of this variable suite, the cross-polarization HV (horizontal send and vertical receive) backscatter was the best single indicator of marsh dieback and recovery. HV backscatter exhibited substantial and significant changes over the dieback and recovery period, tracked measured biomass changes, and significantly correlated with the live/dead biomass ratio. Within the context of regional trends, both HV and VI indicators started higher in pre-dieback marshes and exhibited substantially and statistically higher variability from year to year than that exhibited in the non-dieback marshes. That distinct difference allowed the capturing of the *S. alterniflora* marsh dieback and recovery; however, these changes were incorporated in a regional trend exhibiting similar but more subtle biomass composition changes.

Published by Elsevier Inc.

1. Introduction

1.1. History of marsh diebacks and studies

Salt marshes are essential for terrestrial to ocean energy and nutrient exchanges, storm buffering, maintenance of water quality, and as habitat and nursery for a myriad of wildlife and fish (Cullinan, LaBella, & Schott, 2004; Elmer et al., 2013; Zhang, Ustin, Reimankova, & Sanderson, 1997). Although they perform a critical dynamic role and have intrinsic ecological importance, salt marshes face detrimental pressures from natural and human-induced forces (Belluco et al., 2006; Cullinan et al., 2004; Elmer et al., 2013; Mendelssohn & McKee, 1988; Zhang et al., 1997). Researchers have applied remote sensing monitoring techniques to provide timely and synoptic status and trend information that addresses the spatial heterogeneity and seasonal changes of salt marshes, (Belluco et al., 2006; Cullinan et al., 2004; Elmer et al., 2013; Mendelssohn & McKee, 1988; Wickland, 1991; Zhang et al., 1997). Because biomass production is the primary indicator of salt marsh health, remote sensing activities have focused on changes in biomass composition (e.g., Ramsey & Rangoonwala, 2005; 2006; 2010; Zhang et al., 1997). This paper describes remote sensing applied to the detection and monitoring of *Spartina alterniflora* salt marsh biomass composition changes that revealed the occurrence and recovery of a recently observed phenomenon termed marsh dieback (Elmer et al., 2013; Ramsey & Rangoonwala, 2005; 2006; 2010).

Since the 1960s, *S. alterniflora* (smooth cordgrass) salt marshes that dominate regularly flooded salt marshes of the Atlantic and Gulf coasts of the United States have been documented to experience scattered and irregularly timed periods of browning (chlorotic) leading in most cases to dead marsh and at times marsh loss (Bacon & Jacobs, 2013; Elmer, LaMondia, & Caruso, 2012; Kearney & Riter, 2011; McFarlin, 2012; McKee, Mendelssohn, & Materne, 2004; Mendelssohn & McKee, 1988; Ogburn & Alber, 2006). The driving factors shown to contribute to the dieback include water logging, drought, reduced flushing, herbivory, pathogens, and others (Bacon & Jacobs, 2013; Kearney & Riter, 2011; McFarlin, 2012; McKee et al., 2004; Mendelssohn & McKee, 1988); however, the causes of dieback are likely varied and in most cases remain uncertain (Ogburn & Alber, 2006).

* Corresponding author. Tel.: +1 337 266 8500.
E-mail address: ramseye@usgs.gov (E. Ramsey).

http://dx.doi.org/10.1016/j.rse.2014.07.002
0034-4257/Published by Elsevier Inc.

One of the largest (>100,000 ha) and intensely studied and referenced marsh diebacks occurred in coastal Louisiana between 2000 and 2001 and progressed for up to eight months after discovery (e.g., Bacon & Jacobs, 2013; McKee et al., 2004). Even though the 2000–2001 Louisiana marsh dieback event was large and well-documented, satellite optical remote sensing detected and mapped a marsh dieback in 2008 that dwarfed that event (Ramsey, Werle, Suzuoki, Rangoonwala, & Lu, 2012). In the 2008 dieback, 111,000 ha of fresh and 411,100 ha of salt marshes exhibited moderate to severe marsh dieback within three weeks of Hurricanes Gustav and Ike storm surges impacting the Louisiana coastal region. Also in contrast to all other dieback occurrences, satellite radar remote sensing mapping showed that the dieback was the direct consequence of elevated salinity hurricane storm surges (Ramsey et al., 2012).

1.2. Optical and radar mapping of marsh dieback

The satellite remote sensing detection and mapping of the 2008 dieback event were based on spectral methods developed as part of the 2000 Louisiana dieback study (Ramsey & Rangoonwala, 2005; 2006; 2010). Chance observations leading to early detection of the 2000 dieback provided the opportunity to apply remote sensing techniques to detect the occurrence of marsh dieback and to determine the stage of dieback progression. Pigment concentrations were analyzed at the plant-leaf scale along four transects covering the transition from dead to healthy *S. alterniflora* to determine spectral changes indicative of dieback onset and progression (Ramsey & Rangoonwala, 2005). Those plant-leaf transect results were then extrapolated to the plant-canopy scale in order to simulate aircraft and satellite spatial and spectral resolutions (Ramsey & Rangoonwala, 2006).

Our field studies confirmed the loss of the leaf chlorophyll pigment with marsh dieback noted by McKee et al. (2004) and related the pigment losses to leaf reflectance increases in visible reflectance magnitude, specifically in the blue (400–500 nm), green (500–600 nm) and red (600–700 nm) wavelength bands (Ramsey & Rangoonwala, 2005). The same study showed that although leaf water (spectral determination after Peñuelas & Filella, 1998) and near-infrared (NIR, 700 to 1300 nm) leaf reflectance magnitude decreased with dieback progression, the relationships were weak and only clearly evident at a single late stage marsh dieback site (coefficient of determination, R^2, of 0.35 [leaf water] and 0.72 [NIR], $p < 0.05$) (Ramsey & Rangoonwala, 2005). In order to more fully account for site to site differences in dieback progression, particularly the later stage exhibiting progressive NIR changes, and provide a more reliable satellite remote sensing biophysical measure, vegetation indexes (VI) calculated as the NIR/Green and NIR/Red ratios were applied (Ramsey & Rangoonwala, 2005; 2006). In this study we relied solely on the NIR/Red ratio as the marsh dieback indicator. Although the NIR/Green ratio performed slightly better in earlier stage diebacks, both NIR/Green and NIR/Red were good indicators of dieback progression, and NIR/Red performed better at later stage diebacks at the plant-leaf scale (Ramsey & Rangoonwala, 2005).

The dieback progression explained 0.68 and 0.79 (R^2, $p < 0.10$) and 0.82 and 0.85 (R^2, $p < 0.05$) of the VI leaf-based reflectance variance at the younger and later stage diebacks, respectively (Ramsey & Rangoonwala, 2005). A follow-on study extended the plant-leaf dieback results to the site-specific plant-canopy spectral changes and found that aircraft and satellite remote sensing data could distinguish (1) healthy marsh, (2) live marsh impacted by dieback, and (3) dead marsh, and provide some discrimination of dieback progression (Ramsey & Rangoonwala, 2006). In addition, VI based on the NIR/Red band ratio reproduced hyperspectral plant-canopy indicators of marsh dieback at a 0.88 R^2 (mean square error = 0.21) level (Ramsey & Rangoonwala, 2010). A final mapping of the 2000–2001 dieback event based on six Landsat Thematic Mapper (TM) images collected before and after the dieback onset affirmed the necessity of atmospheric correction and conversion of the remote sensing data to surface reflectance. Further, the TM dieback mapping emphasized that the most convincing evidence of dieback impact or nonimpact is reflected in the temporal pattern of the vegetation index (Ramsey & Rangoonwala, 2010).

In remote sensing of vegetation, even if a pixel contains only a single plant species (with similar leaf spectral properties), natural variability in the background (i.e., substrate, water) and canopy structure, (e.g., the plant orientation and density) along with leaf reflectance are combined into the remote sensing reflectance (e.g., Huete & Jackson, 1988; Jensen & Lorenzen, 1988; Peñuelas & Filella, 1998). The background and structure contributions to the canopy reflectance, which likely have a varied relationship and importance to dieback occurrence or progression, complicate linking of the leaf reflectance to canopy reflectance (Ramsey & Rangoonwala, 2006). Thus, in order to more directly link leaf optical indicators of dieback progression to canopy reflectance, we need to determine indicators that account for or minimize canopy structure and background influences in the canopy reflectance spectra.

While accounting for structure influences in the optical data is challenging, synthetic aperture radar (SAR) mapping is largely directly relatable to the 3-dimensional distribution of water contained within the marsh leaves and stalks and underlying sediment (Dobson, Ulaby, & Pierce, 1995; Ramsey, 1998; Ramsey, 2005). SAR's sensitivity to the 3-D water distribution as represented in the backscatter is illustrated in a mapping application closely related to the marsh dieback and recovery. In that study, the near vertical stalk and leaf orientations increasingly exhibited in the early stages of marsh burn recovery became a denser and taller mix of horizontal and vertical orientations (relative to ground) as the recovery progressed (Ramsey et al., 1999). These changes in preferential orientation and increased density with increasing time-since-burn were tracked with polarimetric SAR (PolSAR) L-band data collected from a P3 Orion aircraft operated by the Naval Warfare Office (Ramsey et al., 1999). Initially, relatively higher VV (vertical send and receive) backscatter reflected the dominantly vertical regrowth. As growth progressed, VV backscatter decreased relative to increased HH (horizontal send and receive) backscatter, and cross polarization, HV and VH, backscatter representing the depolarized horizontal and vertical send radiation (Ramsey, Rangoonwala, Baarnes, & Spell, 2009a; Ramsey et al., 1999). Time-since-burn explained 73% ($p < 0.01$) of the VV/VH power depolarization ratio representing nine marsh burn sites, and the highest single polarization R^2 of 0.83 ($p < 0.01$) was associated with VH backscatter (decibels) (Ramsey, Rangoonwala, Baarnes, & Spell, 2009a; Ramsey et al., 1999). VH was used as an indicator of canopy biomass variance.

Particularly relevant to this study, the single date PolSAR scene predicted the time to complete marsh canopy recovery to be around 1000 (±59) days (Ramsey, Rangoonwala, Baarnes, & Spell, 2009a; Ramsey et al., 1999). In contrast, a single date optical image estimated only 400 to 500 days until complete canopy recovery (Ramsey, Rangoonwala, Baarnes, & Spell, 2009a). It took temporal analyses of nine TM images collected over five years to correctly predict marsh canopy recovery to be around 1000 (±88) days (Ramsey, Sapkota, Baarnes, & Nelson, 2002). A comparison of canopy reflectance and canopy structural measurements collected over three years at one of these marsh sites explains the advantage of SAR over optical monitoring in this case. While the canopy had recovered its stock of live biomass as represented by the optical reflectance spectra and lack of subsequent change after one year of regrowth, the canopy structure differed substantially from a fully mature canopy even after 1.5 years of regrowth (Ramsey, Rangoonwala, Baarnes, & Spell, 2009a). PolSAR's heightened sensitivity to canopy structure as compared to optical imaging should provide additional indicators of marsh dieback that enhance the detection of dieback onset and monitoring of dieback progression, with the additional advantage of radar's all-weather and day-night operability.

1.3. Data collections capturing the 2011 undetected dieback event

In support of yearly summer NASA Uninhabited Aerial Vehicle SAR (UAVSAR) flights over coastal Louisiana in response to the 2010 Macondo-252 oil spill, non-impacted and impacted marsh sites located in the inland coastal zone were monitored nearly concurrently with UAVSAR flights in order to provide comparative baseline data. At two non-oil-impacted *S. alterniflora* marshes, field measures collected as part of this study showed an abrupt change in live to dead biomass from 2010 to 2011. At one site, a portion of the 2010 live marsh remained while at the other site the healthy green marsh of 2010 was completely dead by the summer of 2011. The timing of the 2011 dieback and juxtaposition of these sites with pre- and post-dieback PolSAR and field data collections provided an excellent opportunity to test whether PolSAR data could detect marsh dieback. Although only a limited amount of satellite optical image data was available, this chance finding of marsh dieback also provided a challenging but ideal test of spectral methods developed in the 2000–2001 coastal dieback to detect and map the extent of this undetected dieback event. Together with these testing and validating opportunities is the near coincidental collection post-dieback of co-located PolSAR and field data, and, at one field site, concurrent, co-located optical image data.

1.4. Objectives

Near-coincident collections of field, satellite optical, and UAVSAR PolSAR data during a 2010 to 2012 pre- to post-dieback period of *S. alterniflora* marsh in coastal Louisiana formed the basis for this study, for which the objectives were to (1) document site-specific changes in biomass associated with marsh dieback and recovery using ground based methods; (2) demonstrate the covariance between changes in the optical VI based on the NIR/Red reflectance magnitude ratio and marsh biomass composition; (3) extend the VI based site-specific relationship spatially and temporally with optical satellite data; (4) determine the best single PolSAR based biophysical variable indicator of dieback and recovery based on site-specific biomass relationships; and (5) relate regional changes of VI and the PolSAR based indicator within *S. alterniflora* dieback and non-dieback marshes over the 2010 to 2012 pre- to post-dieback period.

2. Study area

Located in the eastern deltaic plains of the north-central Gulf of Mexico, the study region encompasses estuarine wetlands (Sasser, Visser, Mouton, Linscombe, & Hartley, 2008) that include the 44,447 ha area of interest (AOI) dominated by *S. alterniflora* marsh (Sasser, Visser, Mouton, Linscombe, & Hartley, 2014; Sasser et al., 2008) (Fig. 1). These marshes are scoured by hurricanes that can push water with elevated salinity into inland marshes, causing mortality (Neyland, 2007; Ramsey, Lu, Suzuoki, Rangoonwala, & Werle, 2011; Ramsey, Werle, Lu, Rangoonwala, & Suzuoki, 2009). Channels, levees, and impoundments constructed to provide transport conduits and waterfowl sanctuaries impede overland flow and can lengthen marsh exposure to elevated salinity surge water and, in the case of intense rainfall accompanying storm events, prolong inundation that promotes water logging and subsequent marsh alteration and deterioration (Ramsey, Werle, Lu, Rangoonwala, & Suzuoki, 2009). The combination

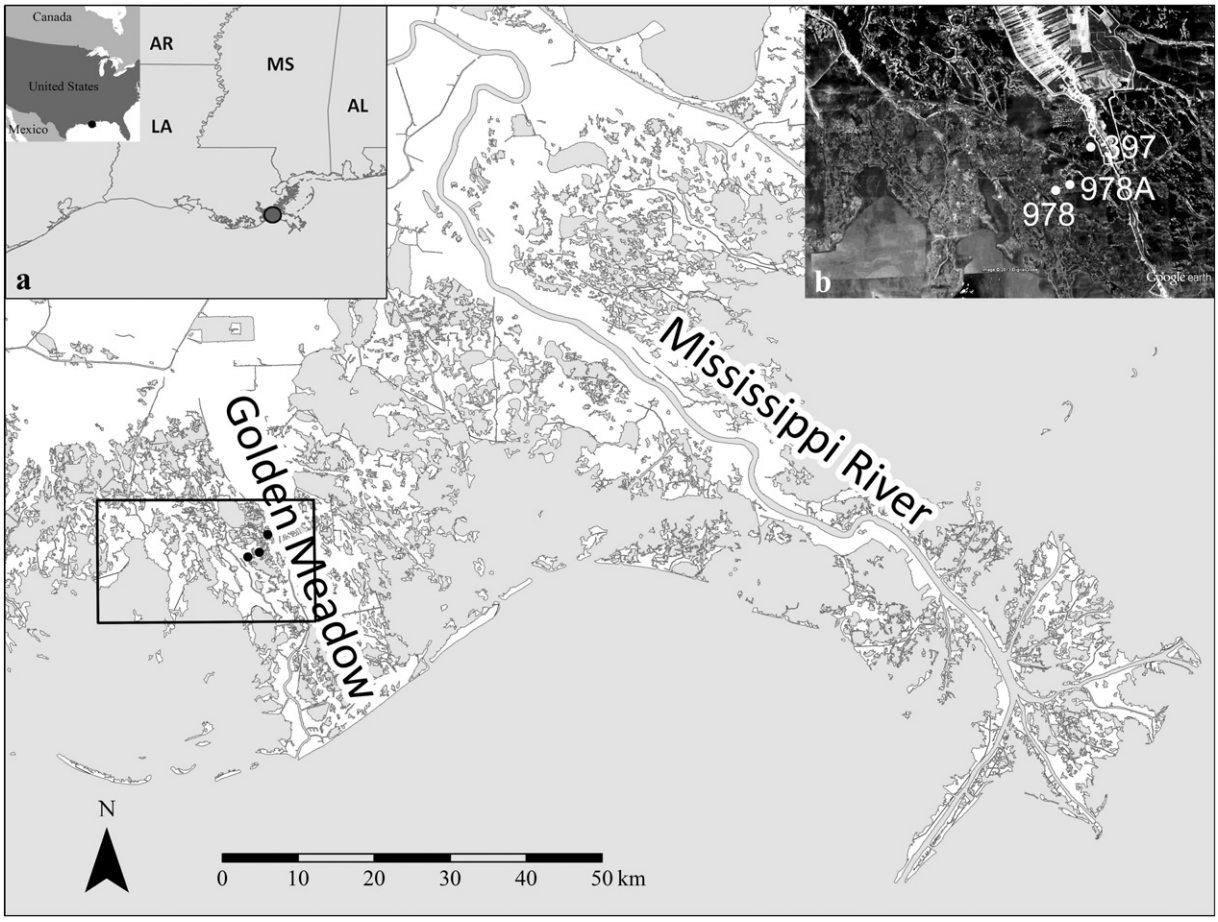

Fig. 1. Location map with study area in Louisiana shown in the insets show a) the location of the study area with respect to the state and b) the location of the field sites in white dots on a Google Earth map.

of low topographic relief, poorly drained soils, subsurface faulting, and flow hindrances creates a spatially complex hydrologic landscape.

3. Methods

3.1. Field measurements

Field data in 2010, 2011, and 2012 were collected within plots at sites 397 and 978 (see Fig. 1 inset b for site locations). Data collection within the 30-m by 30-m plots followed a standard sampling strategy that provides reproducible measures within these structurally variable marshes (for a detailed description see Ramsey, Nelson, Baarnes, & Spell, 2004). Vertical profiles (at a 20-cm increment from the bottom to the top of the canopy) of light attenuation were obtained at a 3-m increment along the 30-m east–west and north–south transects. Biomass was measured by clipping (a few centimeters above the surface) and gathering all standing marsh within a 1-m^2 area chosen to represent the typical marsh at each site. Biomass samples were separated into live and dead portions, dried, and weighed (for method details see Ramsey & Rangoonwala, 2005).

Due to the complete loss of marsh canopy by 2012 at site 978, field and image data collections were obtained at an alternate site 978A close to site 978 (located on Fig. 1). Although there was no expectation that marsh at site 978A was exactly comparable to marsh at site 978 in 2010 and 2011, regional visual reconnaissance suggested marsh at site 978A provided a reasonable surrogate for marsh surrounding site 978 experiencing regrowth in 2012.

At the times of the optical and PolSAR acquisitions, water levels at sites 397 and 978 were obtained from hydrologic stations (within 356 m of sites 397 and 978) operated by the Coastwide Reference Monitoring System as described in the Strategic Online Natural Resources Information System (SONRIS, 2009). Water levels were below the marsh ground surface at the times of all optical image collections but above the ground surface during the UAVSAR overflights. In order to adjust the biomass data to its above water value available for interaction with the incident radar energy, the site average leaf area index (LAI) profile was calculated. The calculation was based on an estimated site canopy vertical light extinction coefficient and the site average light attenuation profile (Decagon Devices, 2006). The site LAI profile was combined with the measured above ground water level to estimate the percent marsh canopy above water and the above water percent was used to adjust the biomass weights to above water biomass. Use of these adjusted biomass metrics offered more accurate depiction of PolSAR based variable and biomass relationships and improved interpretation of relationships when portions of the marsh biomass were submerged.

3.2. Satellite optical image data

The results of the broadband canopy spectral analyses were implemented into the satellite detection and monitoring strategy (Ramsey & Rangoonwala, 2005; 2006). A search of optical satellite image data that individually contained sites 397, 978 and 978A found eight Landsat Enhanced Thematic Mapper Plus (ETM+) (Global Visualization, 2012) and ten SPOT XS 4 and 5 (Earth Explorer, 2012) cloud-free or nearly cloud-free images available for the summer months from 2010 to 2012. After excluding image dates and times where surface marsh flooding and extensive cloud cover were present, two ETM+ images and one SPOT XS 4 image were identified to map the dieback event (Table 1). The Landsat ETM+ has a spatial resolution of 28.5 × 28.5-m and seven spectral bands; blue (0.45–0.52 μm), green (0.52–0.60 μm), red (0.63–0.69 μm), NIR (0.77–0.90 μm), two SWIR (1.55–1.75 μm and 2.09–2.35 μm), and one thermal infrared (10.40–12.50 μm). SPOT XS 4 has a spatial resolution of 20 × 20-m and four spectral bands; green (0.50–0.59 μm), red (0.61–0.68 μm), NIR (0.78–0.89 μm) and one SWIR (1.58–1.75 μm). The ETM+ and SPOT NIR and Red bands were used in the VI calculation.

3.2.1. Conversion to surface reflectance

Data in the three selected images were converted to absolute units (radiance) and a standard radiative transfer atmospheric correction (ATCOR) applied (Richter, 2010; Richter & Schläpfer, 2011). ATCOR required the selection of the scattering phase function and an estimate of the horizontal visibility. The maritime scattering phase function was chosen to best reflect that summer atmospheric composition in subtropical latitudes. To provide an estimate of the horizontal visibility, we first calculated the total atmospheric optical depth as the sum of optical depth related to Mie or aerosol scattering obtained from Multisensor Aerosol Products Sampling System (MAPSS, 2013) and optical depth related to Rayleigh scattering estimated at standard atmospheric conditions (Elterman, 1970). The total optical depth was transformed to horizontal visibility estimates at 0.55 μ (Elterman, 1970; Ramsey & Nelson, 2005). With these inputs, the ATCOR radiative transfer model applied within the PCI image processing software package transformed the at-sensor radiance measurements into marsh canopy reflectance estimates providing fully comparable data across all three image dates (Richter, 2010; Richter & Schläpfer, 2011; PCI Geomatics, 2007).

Only one location provided a check of the performance of the atmospheric correction. The single location visually exhibited a relatively high surface reflectance over the three image dates, and inspection on Google Earth indicated at least a portion of the surface remained non-vegetated. The pixels representing non-vegetated areas were extracted from the Red and NIR image bands for each of the three image dates and the NIR/Red VI calculated for comparison (Table 2).

3.2.2. Image georectification and site-specific vegetation index

The ETM+ and SPOT XS reflectance images were rectified to a Universal Transform Mercator map projection. The image products produced by the rectification were resampled by using bilinear interpolation from the original 28.5 × 28.5-m (ETM+) and 20 × 20-m (SPOT XS) to a common 25 × 25-m pixel spatial resolution.

VI data from SPOT XS 2010 and ETM+ 2011 and 2012 was extracted for sites 397 and 978 using two pixels and four pixels respectively,

Table 1
NASA Uninhabited Aerial Vehicle SAR (UAVSAR), optical satellite images and field data collection dates covering Golden Meadows, Louisiana.

Remote sensing					Ground-based observations	
Sensor	Date of collection	Resolution (m)	Above surface water depth (cm)		Date of collection	
			Site 397	Site 978		
UAVSAR	22 June 2010	5	15.5	11.3	397	8 June 2010
SPOT	30 July 2010	25	−12.3[a]	−10.4[a]	978	15 June 2010
UAVSAR	24 June 2011	5	6.4	21.0	397	2 June 2011
ETM+	15 Aug 2011	25	−4.6[a]	−4.4[a]	978	8 June 2011
UAVSAR	1 July 2012	5	32.3	31.7	397	21 June 2012
ETM+[b]	29 May 2012	25	N/A	0.0	978	21 June 2012

[a] Negative denotes below marsh surface.
[b] Scattered clouds in the image.

Table 2
Surface reflectance and vegetation index (VI) data of a non-vegetated surface.

Year	Green	Red	NIR	Vegetation index (NIR/Red)
2010	20.3 ± 0.85	21.1 ± 0.85	20.3 ± 0.24	0.96 ± 0.05
2011	19.3 ± 0.41	20.2 ± 0.59	21.2 ± 0.13	1.05 ± 0.03
2012	23.6 ± 1.26	24.9 ± 1.51	26.1 ± 0.78	1.05 ± 0.07

The location was chosen because it was non-vegetated and visually exhibited a fairly high surface reflectance. Four pixels (25-m resolution) were used in the surface reflectance and VI average and standard deviation calculations for all three years using SPOT 4 for 2010 and ETM + data for 2011 and 2012.

centered over the field collection areas. These VI data were compared to ground biomass of each site as validation that the satellite image data captured the marsh dieback (Table 3).

3.3. PolSAR data collection and description

The PolSAR data for monitoring the marsh dieback and recovery were made available through NASA's UAVSAR airborne strategic collection in response to the Macondo-252 oil spill and in concern over its possible long term detrimental effects on exposed coastal resources (Jones, Minchew, Holt, & Hensley, 2011; Ramsey, Rangoonwala, Suzuoki, & Jones, 2011). The day and night mapping capabilities offered with radar systems are further extended by the airborne platform offering rapid response in emergencies and agility in tracking time-varying features. UAVSAR's precision repeat-track capability to within 5-m (Jones et al., 2011) enables direct comparison between revisit data collections, and its high transmitted power results in a higher signal-to-noise ratio compared to satellite radars. The high signal-to-noise ratio, a quantity that indicates how much of the measured signal comes from surface backscatter relative to what is generated by noise in the instrument electronics, is particularly important when using HV intensities, which are lower signal level than the HH or VV returns. A previous evaluation of the UAVSAR L-band data found that noise intensities remained below HV backscatter associated with marshes located in the near- to far-range with the possible exception of non-vegetated land covers (Jones et al., 2011; Ramsey, Lu, Suzuoki, Rangoonwala, & Werle, 2011). The L-band 1217.5 to 1297.5 MHz (23.8 cm wavelength) frequency of the SAR system may provide more consistent subcanopy information as suggested in inundation flood mapping (Ramsey, Suzuoki, Rangoonwala, & Bannister, 2013; Ramsey et al., 2012), and its fully polarized or quadrature polarized capability, recording intensities and phases of the HH, VV, and cross-polarization (HV and VH) backscatter, allow a more complete characterization of the scattering properties (McCandless & Jackson, 2004). Each of these unique UAVSAR capabilities can be critically important to monitoring subtle changes associated with marsh dieback in spatially complex land–water landscapes.

In this study, we used UAVSAR's ground range projected, calibrated, and multilooked complex image data referred to as GRD (georeferenced) products (Zheng, Muellerschoen, Michel, Chapman, Hensley & Lou, 2010). These image data reflect the amplitude and phase of the electromagnetic wave measured by the PolSAR sensor representing the complex elements of the scattering matrix (Ramsey, Rangoonwala, Suzuoki, & Jones, 2011). The cross-polarized channels, HV and VH, are combined into a single channel based on the assumption that the HV and VH backscatter is equal for natural surfaces (Van Zyl & Ulaby, 1990). Each GRD image pixel represents ground resolutions of 5.338 m by 6.159 m in the along track (azimuth) and cross track (range) directions, respectively, and an effective number of range and azimuth looks of 3 and 12, respectively. The GRD data were rectified to a UTM map projection at a 5 m by 5 m pixel resolution resulting in a higher spatial sampling of each field site than available with the optical image data. The NASA GRD product provided a readily usable and high fidelity polarimetric data source of high spatial resolution and repeat targeting that enabled direct comparison and detection of subtle changes between the 2010, 2011, and 2012 revisit data collections (Table 1), which was critical for the dieback monitoring.

PolSAR data were extracted at each site by using a 5 by 5 (sites 397 and 978A) and a 7 by 7 (site 978) pixel rectangle centered over the field collection areas (Table 4). The 2010, 2011, and 2012 PolSAR data were used to calculate mean HH, HV (combined HV and VH), and VV backscatter intensities, HH/HV and VV/HV depolarization and HH/VV co-polarization ratios, and the HH–VV phase difference as a measure of the polarization properties of the marsh. In addition, we applied the standard decomposition models (Cloude & Pottier, 1997; Freeman & Durden, 1997) to the complex polarimetric backscatter components of the GRD data in order to categorize the backscatter into distinct mechanisms (e.g., surface, volume, double bounce). Our application of PolSAR data was simplified to the identification of the best single variable, representing polarimetric intensity, intensity ratios, phase difference, or product of decomposition analysis, for determining changes in the marsh canopy associated with dieback and subsequent recovery. These measures should relate directly to the marsh structure and properties, and thus, provide quantifiable measures of change (e.g., Ramsey, Rangoonwala, Suzuoki, & Jones, 2011).

3.4. Dieback extent and recovery

The extent of the dieback was determined by RGB color rendition of pre- (2010) and post-dieback (2011) VI images; 2010 VI as red and 2011 VI as the green and blue (Ramsey, Chappell, & Baldwin, 1997; Ramsey, Rangoonwala, Middleton, & Lu, 2009b). Abnormalities (high differences in reflectance) between the pre- (2010) and post-dieback (2011) VI images would exhibit the pre-dieback color defining the spatial extent of the abnormal VI decrease. Following previous studies, we expected the 2010 color defining the dieback to include the two ground sites where dieback was observed and extend beyond these two site locations to identify the extent of marsh dieback. To transform the dieback color rendition into a quantifiable range of VI magnitudes, we calculated the 2010 minus 2011 VI difference and defined all positive difference as

Table 3
Biomass dry weight measurements and optical data VI (NIR/Red) extracted for the sites 397, 978 and 978A (alternate site for 978 which converted to mud flat in 2012).

Site specific: Biomass (g per m^2)						Remote sensing
Site	Year	Live	Dead	Total	Live/dead	Optical vegetation index (VI)
397	2010	801.2	743.9	1545.1	1.1	4.0 ± 0.17
978	2010	760.9	737.6	1498.5	1.0	3.8 ± 0.30
397	2011	189.7	339.6	529.3	0.6	2.4 ± 0.00
978	2011	7.1	464.1	471.2	0.0	1.5 ± 0.05
397	2012	644.9	418.4	1063.3	1.5	4.2 ± 0.32
978A	2012	579.8	508.6	1088.4	1.1	Cloud cover

At site 978 (not shown) optical VI is 1.3 ± 0.08 for the year 2012.

Table 4
Biomass dry weight measurements and HV backscatter extracted for the sites 397, 978 and 978A (alternate site for 978 which converted to open water in 2012).

Site	Year	Live	Dead	Total	Live/dead	Remote sensing
		Site specific: Biomass (g per m^2) corrected for water depth at the time of the UAVSAR collection[a]				PolSAR
						HV backscatter[b]
397	2010	537.24	498.79	1036.03	1.1	2.40E−03 ± 0.55E−03
978	2010	671.79	651.14	1322.92	1.0	2.49E−03 ± 0.63E−03
397	2011	496.19	177.83	496.19	0.6	4.07E−03 ± 0.85E−03
978	2011	5.35	349.28	354.63	0.0	3.42E−03 ± 0.54E−03
397	2012	244.11	158.40	402.50	1.5	1.41E−03 ± 0.38E−03
978A	2012	163.43	143.37	306.81	1.1	1.37E−03 ± 0.23E−03

[a] Explanation is given in Section 3.1.
[b] At site 978 (not shown), HV backscatter is 2.26E−04 indicating a total loss of canopy by 2012. Recorded water level shows that site was under water at time of UAVSAR collection.

marsh dieback. The resultant dieback bitmap was converted to polygon coverage for ease of comparability between the optical VI and PolSAR HV images (PCI Geomatics, 2007). Similarly, *S. alterniflora* marsh within the study AOI but not in the dieback polygon was included in a non-dieback polygon. A minimum mapping unit of 5 ha was used in the raster to polygon conversions and upland areas and water bodies were not included. The 2011 minus 2012 VI difference was used to portray marsh recovery.

The 2010 to 2011 dieback marsh polygon was used to segment the 2011 to 2012 VI map as well as the PolSAR images into dieback and non-dieback areas for subsequent statistical analyses. These dieback and non-dieback analyses provided a perspective on the observed *S. alterniflora* marsh dieback within a regional and temporal context.

3.5. Documenting change and relationships

Paired two-tailed t-tests (SAS® Enterprise) were conducted to define changes of site-specific field and image-based biophysical measures used to describe changes related to the dieback and recovery. Each t-test first considered the equality of the population variance and then used the appropriate t-test based on the variance equality test and the degrees of freedom (df) and p value reported. Scatter plots were used to show the simple relationships between field biophysical measures and site-specific optical and PolSAR site means in order to extend the field biophysical changes supporting marsh dieback and recovery to the image coverages. Optical site-specific image means were plotted versus the field biophysical measures, while PolSAR site-specific means were plotted versus the field biophysical measures corrected for water depths at the time of the PolSAR collection. Statistical analyses based on the means calculated for the two segments were conducted to test whether differences in the mean responses existed within and between dieback and non-dieback marshes and years for optical VI and PolSAR dieback indicators.

4. Results

4.1. Consistency of the surface reflectance estimates

VIs calculated from Red and NIR reflectance extracted from a single non-vegetated surface location were 0.96, 1.05, and 1.05 in 2010, 2011, and 2012, respectively (Table 2). Even though the exact conditions of the non-vegetated surface are unknown, these results indicate that the atmospheric correction and subsequent NIR/Red band ratio calculation provided a consistent VI representation of the surface condition over the three optical image dates.

4.2. Field data analysis results and relationships to image data

4.2.1. Changes in total, live, and dead biomass

Site photographs showed dramatic changes in canopy condition at sites 397 and 978 from 2010 to 2011 accompanying the marsh dieback (Fig. 2). Biomass measures at both ground sites captured these dramatic changes (Table 3). Total biomass nearly equal in 2010 at sites 397 and 978 had decreased by a factor of three at both sites by 2011. Live biomass had dramatically decreased by 2011 becoming nearly absent at site 978 and reduced to less than one-fourth its 2010 level at site 397. At both sites in 2011, dead biomass was approximately half of its 2010 level (Table 3).

Field measures showed a general recovery of the *S. alterniflora* marshes by 2012; however, marsh at site 978, which was nearly 100%

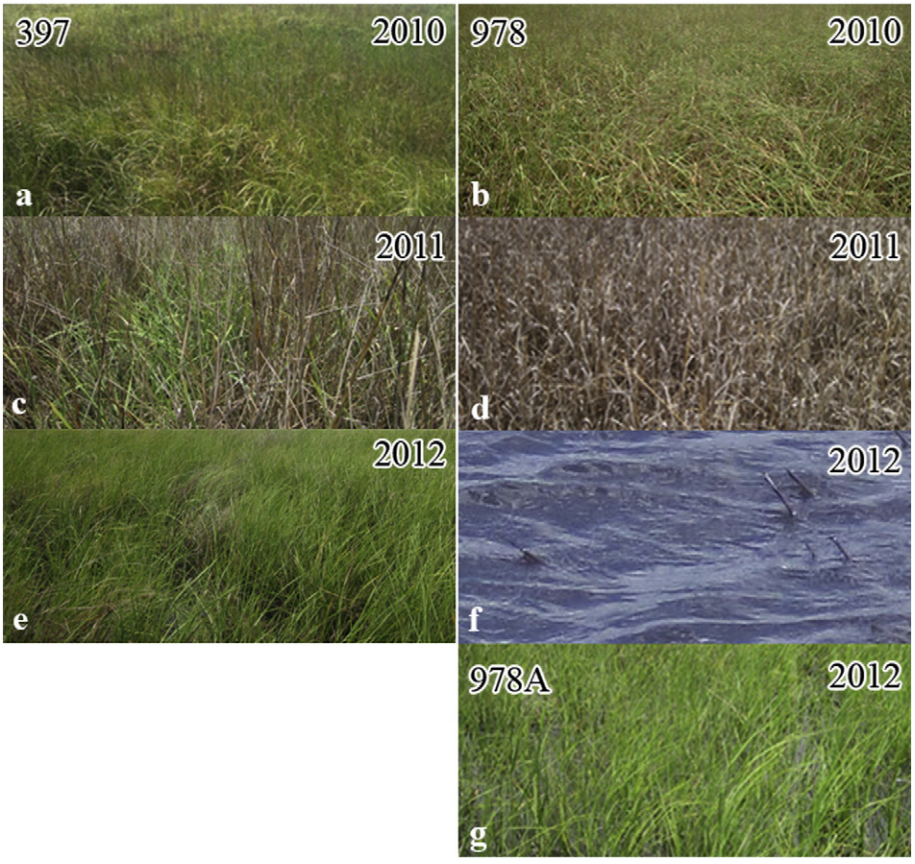

Fig. 2. Site photos obtained in 2010, 2011, and 2012 showing *Spartina alterniflora* marsh at sites 397 (a, c, e) and 978 (b, d, f). Green is live and brown is dead marsh. Because of the conversion of site 978 to mud flat, site 978A (g) representing the same marsh and with generally the same site conditions was substituted.

dead in 2011, was converted to a mud flat with stubble (ca. <10 cm) that was submerged at high tide (Table 3, Fig. 2). In 2012, total biomass at site 397 and at site 978A, representing regrown marsh in the vicinity of site 978, had recovered to two-thirds of their 2010 weights dominantly by an addition of live biomass. The substantially higher increase in live biomass relative to the much smaller addition of dead biomass resulted in the live to dead ratio increasing to above 2010 levels by 2012, particularly at site 397 (Table 3).

4.2.2. Site-specific optical data relationships to field data

VI variance over the three years exhibited high correlations to changes in live biomass, and most specifically, the ratio of live to dead biomass calculated from field data collected at both sites from 2010 to 2012 (Fig. 3, $R^2 = 0.94$, $n = 5$, $p < 0.01$). From 2010 to 2011, there was a decrease in VI (Table 3) at sites 397 ($df = 3$, $p < 0.01$) and 978 ($df = 2$, $p < 0.01$). The 2010 to 2011 VI decrease reflected a decrease in the live to dead ratio accompanied by a decrease in total marsh biomass. From 2011 to 2012, the conversion of marsh to open water at site 978, and the alternate site 978A obscured by clouds, left only 397 field data for comparison to the optical VI data. At site 397, VI dramatically increased from 2011 to 2012 ($df = 2$, $p < 0.01$) returning to nearly the 2010 pre-dieback VI value ($df = 3$, $p < 0.01$). The VI increase reflected an increase in biomass dominated by the live biomass contribution (Table 3).

4.2.3. Site-specific PolSAR data relationships to field data

Biomass was corrected for the submerged portion based on the water level at the times of the PolSAR collections (Tables 1 and 4). Of all the bivariate correspondences between the above-water-surface biomass and the PolSAR based variables, HV backscatter and live/dead biomass exhibited the highest explanatory relationship (Fig. 4, $R^2 = 0.85$, $n = 6$, $p < 0.01$). In addition, although a number of PolSAR based variables covaried with changes in the above-water surface total biomass, the cross-polarization backscatter (represented by HV) when normalized by total co-polarization backscatter provided one of the highest explanatory relationships to percent biomass above water (Fig. 5, $R^2 = 0.95$, $n = 6$, $p < 0.01$).

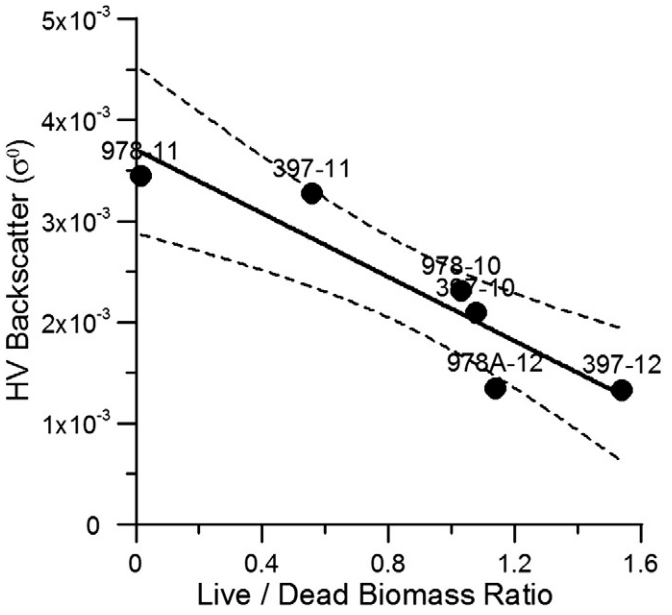

Fig. 4. The negative relationship between HV backscatter and the canopy above water live/dead biomass composition at each field site over the three collection years provided the highest explanatory relationship $R^2 = 0.84$, $n = 6$, $p < 0.01$.

In marsh surrounding site 397, HV backscatter increased from 2010 to 2011 ($df = 48$, $p < 0.01$) and decreased from 2011 to 2012 ($df = 33$, $p < 0.01$). The same trend was reflected for marsh within the vicinity of site 978 (978A substituted for 978 in 2012) with a HV backscatter increase from 2010 to 2011 ($df = 47$, $p < 0.01$) and subsequent decrease to 2012 ($df = 33$, $p < 0.01$). In 2012, HV backscatter was the lowest measured in all three years (Table 4). The high correlation of HV backscatter with biomass and its tracking of changes in total above water biomass provide confidence that the 2010 to 2011 change in HV backscatter was associated with changes brought about by the dieback event. The high water and resultant sizeable loss of the lower canopy contribution in 2012 raises concern about the relevancy of 2011 to 2012 HV backscatter decrease. Its sensitivity to the biomass percent

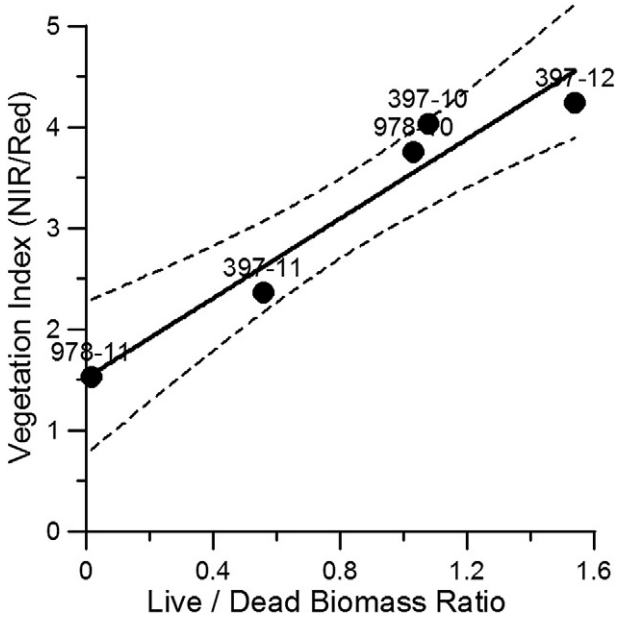

Fig. 3. The positive relationship exhibited high correlation between VI and the canopy live/dead biomass composition at each field site over the three collection years ($R^2 = 0.94$, $n = 5$, $p < 0.01$).

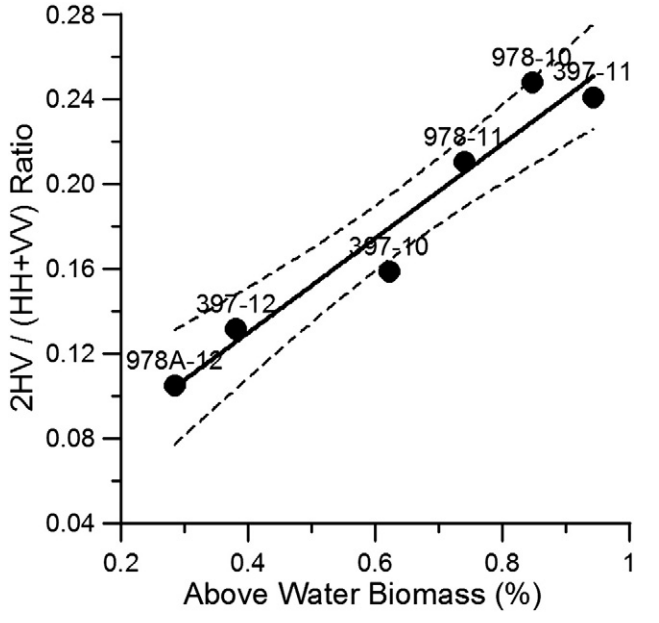

Fig. 5. The cross- and co-polar backscatter ratio related to the percent of canopy total biomass remaining above the water level at each field site at the time of the UAVSAR overflights. This variable provided the highest explanatory relationship to percent biomass above water $R^2 = 0.95$, $n = 6$, $p < 0.01$.

remaining above water, however, indicates that at least part of the HV backscatter was not a function of the changing portions of submerged biomass and was instead associated with the marsh recovery.

4.2.4. Site-specific VI and HV relationship

The final appraisal of HV backscatter as an indicator of marsh dieback, and particularly, as an indicator of marsh dieback recovery was conducted by comparison of the correlation of HV backscatter and VI changes reflecting the 2010 to 2011 dieback and 2011 to 2012 recovery (Fig. 6, $R^2 = 0.89$, $n = 5$, $p < 0.01$).

4.3. VI changes in dieback and non-dieback marshes

The AOI area was segmented into *S. alterniflora* dieback (6649.9 ha) and the non-dieback (11,642.4 ha) marsh polygons discussed in Section 3.4. The 2010 to 2011 VI decrease in *S. alterniflora* and a subsequent recovery of those marshes from 2011 to 2012 were also shown by running t-tests (Fig. 7a and b). The mean VI of pixels contained within the dieback polygon decreased from 2.67 in 2010 to 1.73 in 2011 ($df = 1.23 \times 10^5$, $p < 0.01$) and subsequently increased to 2.87 by 2012 ($df = 1.09 \times 10^5$, $p < 0.01$). Non-dieback marsh VI meansincreased slightly from 2.19 in 2010 to 2.24 in 2011 ($df = 4.34 \times 10^5$, $p < 0.01$) and exhibited a more substantial increase to 2.78 in 2012 ($df = 3.15 \times 10^5$, $p < 0.01$). Differences calculated from 2010 to 2011 and 2012 to 2011 were 0.971 and 1.01 for dieback VIs ($df = 1.89 \times 10^5$, $p < 0.01$), respectively, and 0.001 and 0.514 for non-dieback VIs ($df = 3.82 \times 10^5$, $p < 0.01$), respectively.

4.4. HV changes in dieback and non-dieback marshes

Marsh dieback was calculated as the 2010–2011 difference (Fig. 8a), and marsh recovery as the 2011–2012 difference in the HV backscatter (Fig. 8b) (Table 4). The mean HV backscatter of pixels contained within the dieback polygon increased from 3.06×10^{-3} in 2010 to 4.21×10^{-3} in 2011 ($df = 3.73 \times 10^6$, $p < 0.01$) and subsequently decreased to 1.91×10^{-3} by 2012 ($df = 3.73 \times 10^6$, $p < 0.01$). Non-dieback marsh pixels increased moderately from 2.34×10^{-3} in 2010 to 2.88×10^{-3} in 2011 ($df = 6.59 \times 10^6$, $p < 0.01$) and exhibited a substantial decrease to 2.11×10^{-3} in 2012 ($df = 6.23 \times 10^6$, $p < 0.01$). Differences calculated from 2010 to 2011 and 2012 to 2011 were -1.18×10^{-3} and -2.37×10^{-3} for dieback HVs ($df = 3.67 \times 10^6$, $p < 0.01$), respectively, and -0.55×10^{-3} and -0.811×10^{-3} for non-dieback HVs ($df = 6.47 \times 10^6$, $p < 0.01$), respectively.

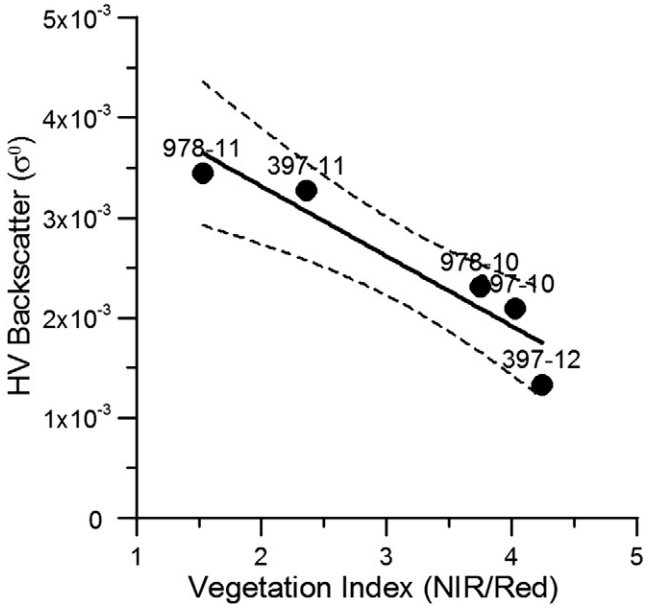

Fig. 6. The negative correspondence between HV backscatter and VI at the two field sites over the three study years. This depiction proved HV as an indicator of marsh dieback recovery which could be used as a VI equivalent proxy ($R^2 = 0.89$, $n = 5$, $p < 0.01$).

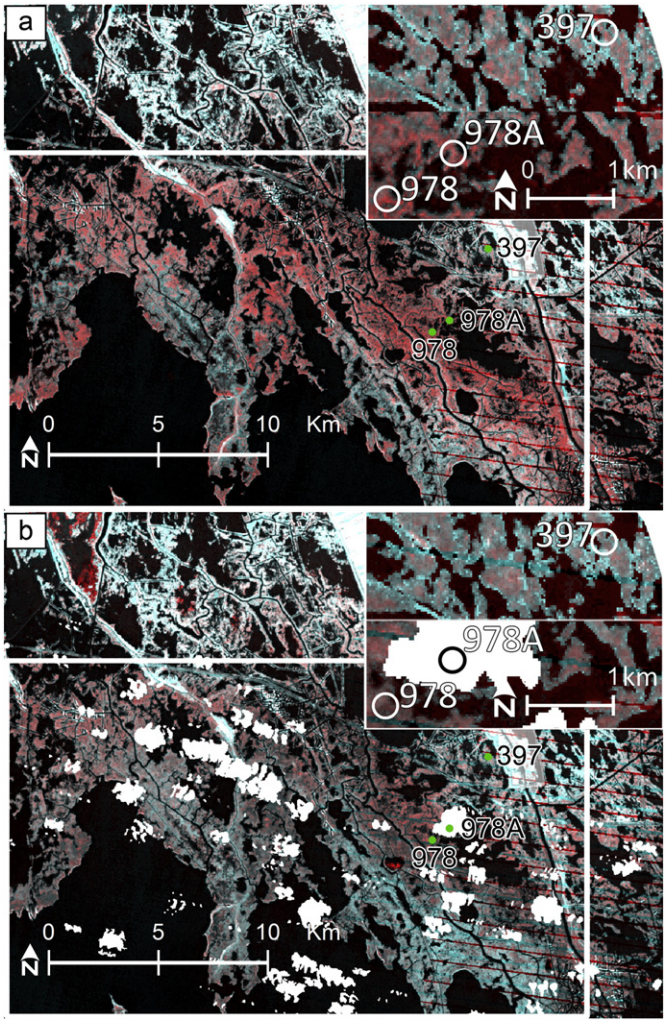

Fig. 7. a) RGB color rendition of pre- (2010) and post-dieback (2011) VI images, 2010 VI was rendered as red and 2011 VI as the green and blue. The red tone illustrates the extent of marsh dieback and bluish tones the non-dieback marshes. b) The 2012 VI was rendered as red and 2011 VI as the green and blue. The red tone illustrates the extent of marsh recovery. Even though of lower contrast, the pattern of red hues represents the 2011 to 2012 VI increase indicating a marsh recovery. Water (in black), upland and clouds (in 2012 ETM+ image) (in white) were excluded from all VI analyses. The inset locates the field sites. The white box outlines the AOI.

5. Discussion

Field and satellite optical data conclusively revealed and mapped a dieback that occurred between the summers of 2010 and 2011 and the following 2012 recovery in the *S. alterniflora* marshes of coastal Louisiana. Although previous studies established marsh dieback biophysical indicators amenable to remote sensing, a shortcoming in mapping the 2000–2001 and 2008 dieback events was the lack of concurrent field and image data collections before and after each event (Ramsey & Rangoonwala, 2005; 2006; Ramsey et al., 2012). In this study, biomass changes were directly measured before and one year after the dieback event. These field measures captured the dramatic decrease in biomass and live to dead biomass composition accompanying the 2010 to 2011 dieback, the reversal of biomass composition signifying a recovery progression by 2012 (Table 3), and a dramatic conversion of healthy marsh

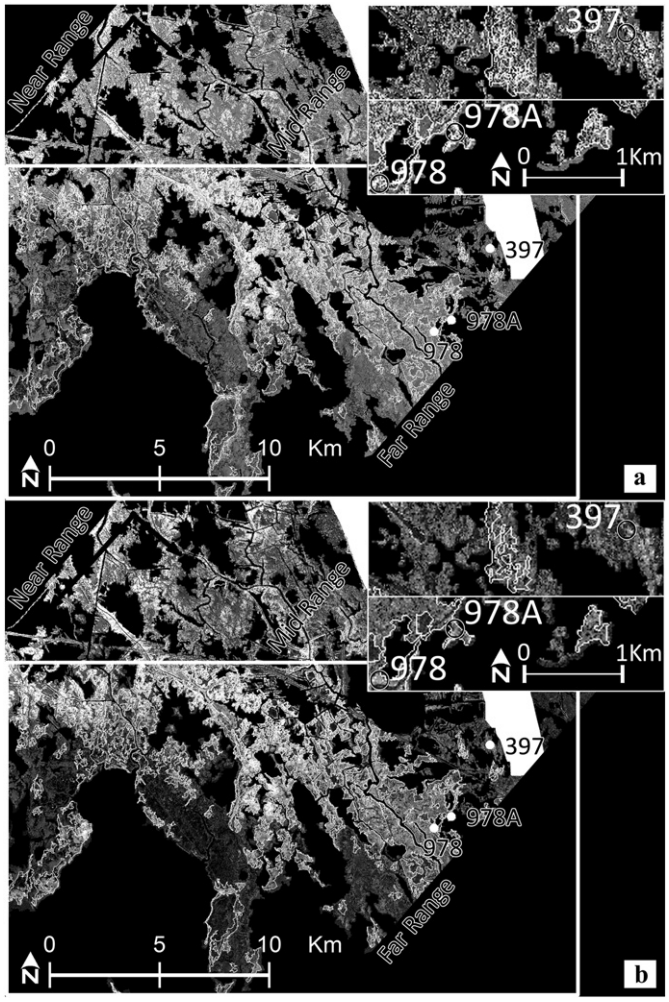

Fig. 8. UAVSAR HV backscatter a) 2010 and 2011 difference image and b) 2012 and 2011 difference image overlain with the VI dieback polygon vector (in white). The lighter gray tone depicts the extent of marsh dieback (and subsequent recovery) and dark gray non-dieback marshes. Water (in black) and upland (in white) were excluded from all HV analyses. The insets show field site locations. The white box outlines the AOI.

in 2010 to mud flat by 2012 (Fig. 2, Table 3). The documentation of biophysical changes accompanying the dieback and recovery progression and dramatic marsh loss provides unique insight into the mechanism of marsh dieback and loss, and establishes what biophysical changes remote sensing methods could reliably monitor to detect and map the dieback progression.

Results of this study reinforced the utility of optical VI based on the NIR/Red ratio to map marsh diebacks (Ramsey, Lu, Suzuoki, Rangoonwala, & Werle, 2011; Ramsey & Rangoonwala, 2005; Ramsey & Rangoonwala, 2006). Those previous studies applied transect strategies and direct mapping of elevated salinity surge waters to link VI changes to dieback onset and progression. In this study, near-concurrent collection of biophysical and satellite data in concert with the marsh transition from healthy to dieback to recovery provided the capability for direct covariance analyses. As indicated in the previous VI dieback mapping and substantiated in numerous remote sensing studies that mapped biomass with a variety of near-infrared and visible band ratios (He, Guo, & Wilmshurst, 2007; Huete, Justice, & Leeuwen, 1999; Vogelmann, Rock, & Moss, 1993), we found that the live biomass component dominantly influences the VI variance (Fig. 3, Table 3). These results provide conclusive evidence that the remote sensing VI is a direct indicator of marsh biophysical changes defining dieback and recovery.

Site-specific biophysical and VI relationships extended regionally by using three consecutive years of satellite optical image data showed that biomass composition as represented by optical-based VI magnitude varied spatially but the yearly pattern of change was not spatially consistent throughout the *S. alterniflora* marshes. The two field sites were encompassed within a nearly contiguous 6649.9 ha of marsh that exhibited the dieback and recovery pattern of VI decrease and subsequent increase. Outside this dieback marsh region, however, 11,642.4 ha of surrounding non-dieback marsh did not exhibit the dieback VI pattern; this was also supported by the statistical results.

Regional analyses found that from 2010 to 2011 dieback marshes had a substantial average VI decrease compared to practically no change in non-dieback marshes. By 2012, VI increased in dieback marshes to nearly pre-dieback VI magnitudes and non-dieback marshes had a VI increase about half that. Basically, the 2010 to 2011 dieback and non-dieback marsh difference in VI decrease was the single factor that identified the dieback. That decrease difference, however, began from different starting points. On average, VI was nearly 0.5 units higher in pre-dieback marsh than in non-dieback marsh in 2010. The nearly 2-fold higher VI increase in 2012 in dieback marshes compared to non-dieback marshes brought the VI levels, and by extension, the live biomass composition levels into near alignment. To determine whether the initial VI difference was a precursor to the dieback onset, however, was not part of this study. What was determined was that VI mapping captured a dieback event including eventual marsh loss that differentially occurred in *S. alterniflora* marshes exhibiting higher pre-dieback VIs than non-dieback marshes.

Assessment of the PolSAR based single variable and biomass measures adjusted for above-surface-water levels found that HV backscatter provided the best single variable indicator of biomass changes accompanying marsh dieback and recovery. HV backscatter as an indicator of depolarization of the co-polarized data (HH and VV) originates mainly from multiple scattering within the canopy and has reported sensitivity to forest and agriculture biomass (Brakke, Kanemasu, & Steiner, 1981; Ferrazzoli et al., 1997; Ghasemi, Sahebi, & Mohammadzadeh, 2011; Westman & Paris, 1987). L-band backscatter is sensitive to grassland biomass (Dobson, Pierce, & Ulaby, 1996), and studies have demonstrated direct correspondence between L-band polarimetric radar HV backscatter and grassland biomass measures. Dabrowska-Zielinska et al. (2014) found strong per-class linear relationships between the canopy Leaf Area Index, a proxy of biomass, and HV backscatter. Herold, Schmullius, and Hajnsek (2001) found that of the three polarizations HV backscatter provides the highest sensitivity to grassland canopy features and the highest explanation of plant water content (an indicator of live biomass). Results of those studies concur with results reported here that indicate the potential of HV backscatter to provide grassland biomass information. However, the nature of its relationship to changes in herbaceous (grasses) land cover remains less clear than for the more fully studied forest and agriculture landcovers.

Another factor is the influence of decreased above-water biomass. As seen in Table 4, HV backscatter from surface water covering marsh stubble (site 978 in 2012) was over six times lower than HV backscatter from site 978A with only 28% of its total biomass weight of nearly 1.1 kg exposed. Even with a majority of the marsh canopy submerged, above water biomass produced an appreciable increase in the cross-polarized HV backscatter. Further, HV backscatter magnitude was similar at site 397 in 2012, and in 2011, both sites 397 and 978 exhibited dramatically higher HV backscatter with comparable total biomass quantities. It is likely that some portion of the 2011 to 2012 decrease in HV backscatter was related to the change in live biomass composition representing marsh recovery.

HV backscatter extracted from sites 397 and 978 (978A) changed significantly from year to year (Table 4). Somewhat counterintuitively because of its expected positive relationship with canopy density, HV backscatter increased with the decrease in marsh biomass 2010 to 2011 and decreased with regrowth from 2011 to 2012. Following

this negative relationship with canopy dieback and regrowth, HV backscatter exhibited a significant negative correlation with live biomass composition (Fig. 6). Ongoing analyses are pursuing specific details concerning the nature of HV backscatter correspondence with biophysical changes accompanying the marsh dieback. However, even if not yet fully explained, site-specific evidence of substantial changes in accordance with the dieback and recovery pattern and its correspondence with changes in live biomass is strong even though inferential.

Average HV backscatter within the dieback marshes showed a substantial increase from 2010 to 2011 and a dramatic reversal from 2010 to 2011. HV backscatter also increased in non-dieback marshes from 2010 to 2011 but by less than half the amount of dieback marshes. The HV backscatter decrease in non-dieback marshes was more substantial from 2011 to 2012 but still only a third of the change in dieback marshes. HV backscatter started out higher in the dieback marshes in 2010 but the dieback and non-dieback marshes ended in 2012 with similar average HV backscatter magnitudes. The overall pattern of change, although negatively correlated, tracked the VI pattern. Although a small change from 2010 to 2011 and even a more substantial from 2011 to 2012 occurred, the change in non-dieback marshes is still small in comparison to those in dieback marshes.

Both VI and HV backscatter show different starting points in the two marshes in 2010 and more dramatic changes of their values from 2010 to 2011 and again from 2011 to 2012 in dieback as compared to non-dieback marshes. Individually, VI and HV ended nearly equal in the two marshes by 2012. Changes in VI are substantiated to track changes in marsh live biomass composition as a direct indicator of dieback. While not all changes in live biomass composition define a dieback event, the dramatic biomass changes shown to be in accordance with VI site-specific changes proved that VI mapping based on satellite SPOT XS and Landsat ETM + image data captured an undetected and extensive region of *S. alterniflora* dieback. HV backscatter tracked live biomass composition and VI site-specific changes and closely emulated VI dieback and non-dieback marsh regional patterns. The higher variability of VI and HV backscatter within the defined dieback marshes as compared to the non-dieback marshes may provide the pattern that identifies these events.

6. Conclusion

VI changes based on satellite SPOT and ETM + image data transformed to surface reflectance and validated by site-specific measurements detected and mapped a sizeable (6649.4 ha) and undetected *S. alterniflora* marsh dieback event in coastal Louisiana between 2010 and 2012. The VI changes were shown to directly co-vary with field-measured changes in the live biomass composition, and the live biomass composition to represent changes in the marsh canopy related to dieback and its recovery. While not all changes in live biomass composition define a dieback event, dramatic biomass changes accepted as indicators of dieback were confirmed to be in accordance with VI site-specific changes. These results reinforce the established utility of optical VI to map marsh diebacks. The detection and mapping of a sizeable and undetected sudden marsh dieback event establish the capability of moderate spatial resolution satellite optical data to provide critical coastal resource status and trend information that is not always obtainable by field observations or intermittent aerial photographic surveys.

The juxtaposition of the NASA UAVSAR PolSAR data collections for the three summers that encompassed the dieback was used to demonstrate the correlation among the field, optical, and PolSAR data sources and their relationship to the marsh dieback and recovery. We found that the single best PolSAR based indicator of marsh dieback and recovery was the cross-polarized (HV) backscatter. HV backscatter exhibited substantial and significant changes over the dieback and recovery period tracking changes in biomass, represented as changes in the live biomass composition. As in VI, HV backscatter significantly correlated, although negatively, to changes in live and dead biomass ratio.

VI and HV backscatter exhibited similar initial and change patterns within and between *S. alterniflora* dieback and non-dieback marshes. Initial starting points for each were higher in the dieback marshes and VI as well as HV backscatter means calculated for the 2012 dieback and non-dieback marshes were similar. Overall, the dieback marshes were associated with and detected by substantially higher changes as compared to the much more subtle but largely similar pattern of changes occurring in non-dieback marshes. The possibility that dramatic biophysical changes accompanying dieback events can be encased within spatially extensive regional trends similar in pattern but much more subtle is a critical result of this study. Along with the capture of an extensive and undetected dieback with satellite optical data, another critical result of this study is that radar based image data may provide direct mapping of marsh dieback.

Work is ongoing particularly in specifying the HV backscatter relationship to canopy composition and influences of flooding; however, results of this study demonstrate a high potential for nearly all-weather and day and night operable SAR systems like the targeted, high fidelity, high signal to noise and high spatial resolution UAVSAR PolSAR system to identify canopy structure changes that may portend damaging dieback events. Targeted PolSAR and optical imaging could advance both the canopy biophysical detail and mapping consistency necessary for capturing heightened changes within a pattern of regional changes.

Acknowledgement

We thank Francis Fields Jr. of the Apache Louisiana Minerals LLC, a subsidiary of Apache Corporation, for access to their properties. We also thank Ryan Longhenry, Data Management Specialist, U.S. Geological Survey (USGS), Earth Resources Observation and Science (EROS) Center and Carolyn Gacke, contractor Science Applications International Corporation at USGS EROS Center for the help and support in providing the SPOT satellite data. We appreciate the help by Sijan Sapkota of the U.S. Geological Survey for his assistance in developing statistical models. We appreciate the review of the manuscript by John Iiames, Research Biologist at U.S. Environmental Protection Agency, and Dirk Werle of AERDE Environmental Research, Canada. We also thank the two anonymous reviewers for their exhaustive, judicious and perceptive reviews. Research was supported in part by National Aeronautics Space Administration (NASA) grant #11-TE11-104 and was carried out in collaboration with the Jet Propulsion Laboratory, California Institute of Technology, under a contract with NASA. Any use of trade, firm, or product names is for descriptive purposes only and does not imply endorsement by the U.S. Government.

References

Bacon, C., & Jacobs, A. (2013). Sudden wetland dieback in Delaware's inland bays. (URL). http://deestuaryarchive.mobiusnm.com/scienceandresearch/Science_Conf/Conference_Presentations/DESC07_No16_Bason.pdf (accessed: 18 March 2013).

Belluco, E., Camuffo, M., Ferrari, S., Modenese, L., Silvestri, S., Marani, A., et al. (2006). Mapping salt-marsh vegetation by multispectral and hyperspectral remote sensing a. *Remote Sensing of Environment, 105*, 54–67.

Brakke, T., Kanemasu, E., & Steiner, J. (1981). Microwave radar response to canopy moisture, leaf-area index, and dry weight of wheat, corn and sorghum. *Remote Sensing of Environment, 11*, 207–220.

Cloude, S., & Pottier, E. (1997). An entropy based classification scheme for land applications of polarimetric SAR. *IEEE Transactions on Geoscience and Remote Sensing, 35*, 68–78.

Cullinan, M., LaBella, N., & Schott, M. (2004). Salt marshes — A valuable ecosystem. *The Traprock, 3*, 20–23.

Dabrowska-Zielinska, K., Budzynska, M., Tomaszewska, M., Bartold, M., Gatkowska, M., Malek, I., et al. (2014). Monitoring wetlands ecosystems using ALOS PALSAR (L-Band, HV) supplemented by optical data: A case study of Biebrza wetlands in northeast Poland. *Remote Sensing, 6*(2), 1605–1633.

Devices, Decagon (2006). *Operators manual; AccuPAR model LP-80 PAR/LAI ceptometer*. Pullman, WA: Decagon Devices, Inc.

Dobson, C., Pierce, L., & Ulaby, F. (1996). Knowledge-based land-cover classification using ERS-1/JERS-1 SAR composites. *IEEE Transactions on Geoscience Remote Sensing, 34*(1), 83–99.

Dobson, C., Ulaby, F., & Pierce, L. (1995). Land-cover classification and estimation of terrain attributes using synthetic aperture radar. *Remote Sensing of Environment*, *51*, 199–214.

Elmer, W., LaMondia, J., & Caruso, F. (2012). Association between *Fusarium* spp. on *Spartina alterniflora* and dieback sites in Connecticut and Massachusetts. *Estuaries and Coasts*, *35*, 436–444.

Elmer, W., Useman, S., Schneider, R., Marra, R., LaMondia, J., Mendelssohn, I., et al. (2013). Sudden vegetation dieback in Atlantic and gulf coast salt marshes. *Plant Disease*, *97*(4), 436–445.

Elterman, L. (1970). *Vertical-attenuation model with eight surface meteorological ranges 2 to 13 kilometers*. Air Force Cambridge Research Laboratories (AFCRL-70-0200, 56p).

Earth Explorer (2012). *U.S. Geological Survey*. (URL) http://earthexplorer.usgs.gov (accessed 11 November 2012).

Ferrazzoli, P., Paloscia, S., Pampaloni, P., Schiavon, G., Sigismondi, S., & Solimini, D. (1997). The potential of multifrequency polarimetric SAR in assessing agricultural and arboreous biomass. *IEEE Transactions on Geoscience and Remote Sensing*, *35*(1), 5–17.

Freeman, A., & Durden, S. (1997). A three component scattering model for polarimetric SAR data. *IEEE Transactions on Geoscience and Remote Sensing*, *36*, 963–973.

Ghasemi, N., Sahebi, M., & Mohammadzadeh, A. (2011). A review on biomass estimation methods using synthetic aperture radar data. *International Journal of Geomatics and Geosciences*, *1*(4), 776–788.

Global Visualization (2012). *U.S. Geological Survey*. (URL) http://glovis.usgs.gov (accessed: 10 October 2012).

He, Y., Guo, X., & Wilmshurst, J. F. (2007). Comparison of different methods for measuring leaf area index in a mixed grassland. *Canada Journal of Plant Science*, *87*, 803–813.

Herold, M., Schmullius, C., & Hajnsek, I. (2001). Multifrequency and polarimetric radar remote sensing of grassland — Biophysical and landcover parameter retrieval with E-SAR data. In M. F. Buchoithner (Ed.), *A decade of trans-European remote sensing cooperation* (pp. 95–101). CRC Press.

Huete, A.R., & Jackson, R. (1988). Soil and atmosphere influence on the spectra of partial canopies. *Remote Sensing of Environment*, *25*, 89–105.

Huete, A.R., Justice, C., & Leeuwen, W. (1999). MODIS vegetation index (MOD 13) algorithm theoretical basis document version 3. (URL) http://modis.gsfc.nasa.gov/data/atbd/atbd_mod13.pdf (accessed: 18 June 2013).

Jensen, A., & Lorenzen, B. (1988). Reflectance of blue, green, red and near infrared radiation from wetland vegetation used in a model discriminating live and dead above ground biomass. *New Phytologist*, *108*, 345–355.

Jones, C. E., Minchew, B., Holt, B., & Hensley, S. (2011). Studies of the deepwater horizon oil spill with the UAVSAR radar, monitoring and modeling of the deepwater horizon oil spill. In Y. Liu, A. Macfadyen, Z. -G. Ji, & R. H. Weisberg (Eds.), *A record-breaking enterprise, American Geophysical Monograph Series* (pp. 33–50). Washington, DC: American Geophysical Union.

Kearney, M. S., & Riter, J. C. A. (2011). Inter-annual variability in Delaware Bay brackish marsh vegetation, USA. *Wetlands Ecology and Management*, *19*, 373–388.

MAPSS (2013) (). Multi-sensor aerosol products sampling system. http://giovanni.gsfc.nasa.gov/mapss/#location=Stennis (accessed: 20 July 2013)

McCandless, S., Jr., & Jackson, C. (2004). Principals of synthetic aperture radar. In Christopher Jackson, & John Apel (Eds.), *Synthetic aperture radar marine user's manual* (pp. 1–24). U.S. Department of Commerce.

McFarlin, C. R. (2012). *Salt marsh dieback 2012: The response of Spartina alterniflora to disturbances and the consequences of marsh invertebrates.* (PhD dissertation). Athens, Georgia: University of Georgia (238 pp.).

McKee, K. L., Mendelssohn, I. A., & Materne, M.D. (2004). Acute salt marsh dieback in the Mississippi River deltaic plain: A drought-induced phenomenon? *Global Ecology and Biogeography*, *13*, 65–73.

Mendelssohn, I. A., & McKee, K. L. (1988). *Spartina alterniflora* die-back in Louisiana: Time-course investigation of soil waterlogging effects. *Journal of Ecology*, *76*, 509–521.

Neyland, R. (2007). The effects of hurricane Rita on the aquatic vascular flora in a large fresh-water marsh in Cameron Parish, Louisiana. *Castanea*, *72*, 1–7.

Ogburn, M., & Alber, M. (2006). An investigation of salt marsh dieback in Georgia using field transplants. *Estuaries and Coasts*, *29*, 54–62.

Peñuelas, J., & Filella, L. (1998). Visible and near-infrared reflectance techniques for diagnosing plant physiological status. *Trends in Plant Science*, *3*(4), 151–156.

PCI Geomatics (2007). *Geomatica SPW 10.1 user guide (SAR Polarimetry Workstation)*. ON, Canada: PCI Geomatics Enterprises, Inc, Richmond Hill 179 p.

Ramsey, E., III (1998). Radar remote sensing of wetlands. In R. Lunetta, & C. Elvidge (Eds.), *Remote Sensing Change Detection: Environmental Monitoring Methods and Applications* (pp. 211–243). Ann Arbor Press, Inc: Michigan.

Ramsey, E., III (2005). Remote sensing of coastal environments. In M. L. Schwartz (Ed.), *Encyclopedia of coastal science, encyclopedia of earth sciences series* (pp. 797–803). The Netherlands: Kluwer Academic Publishers.

Ramsey, E., III, Chappell, D., & Baldwin, D. (1997). AVHRR imagery used to identify hurricane Andrew damage in a forested wetland of Louisiana. *Photogrammetric Engineering and Remote Sensing*, *63*, 293–297.

Ramsey, E., III, Lu, Z., Suzuoki, Y., Rangoonwala, A., & Werle, D. (2011). Monitoring duration and extent of storm surge flooding along the Louisiana coast with Envisat ASAR data. *IEEE Journal of Selected Topics in Earth Observations and Remote Sensing*, *4*, 387–399.

Ramsey, E., III, & Nelson, G. (2005). A whole image approach for transforming EO1 Hyperion hyperspectral data into highly accurate reflectance data with site-specific measurements. *International Journal of Remote Sensing*, *26*, 1589–1610.

Ramsey, E., III, Nelson, G., Baarnes, F., & Spell, R. (2004). Light attenuation profiling as an indicator of structural changes in coastal marshes. In R. Lunetta, & J. Lyon (Eds.), *Remote sensing and GIS accuracy assessment* (pp. 59–73). New York: CRC Press.

Ramsey, E., III, Nelson, G., Sapkota, S., Laine, S., Verdi, J., & Krasznay, S. (1999). Using multiple polarization L band radar to monitor marsh burn recovery. *IEEE Transactions on Geoscience and Remote Sensing*, *37*, 635–639.

Ramsey, E., III, & Rangoonwala, A. (2005). Leaf optical property changes associated with the occurrence of *Spartina alterniflora* dieback in coastal Louisiana related to remote sensing mapping. *Photogrammetry Engineering and Remote Sensing*, *71*, 299–311.

Ramsey, E., III, & Rangoonwala, A. (2006). Site-specific canopy reflectance related to marsh dieback onset and progression in coastal Louisiana. *Photogrammetry Engineering and Remote Sensing*, *72*, 641–652.

Ramsey, E., III, & Rangoonwala, A. (2010). Mapping the onset and progression of marsh dieback. In Y. Wang (Ed.), *Remote sensing of coastal environments* (pp. 123–149). New York: CRC Press, Taylor & Francis.

Ramsey, E., III, Rangoonwala, A., Baarnes, F., & Spell, R. (2009a). Mapping fire scars and marsh recovery with remote sensing image data. In X. Yang (Ed.), *Remote sensing and geospatial technologies for coastal ecosystem assessment and management, lecture notes in geoinformation and cartography* (pp. 415–438). Springer-Verlag Berlin Heidelberg.

Ramsey, E., III, Rangoonwala, A., Middleton, B., & Lu, Z. (2009b). Satellite optical and radar image data of forested wetland impact on and short-term recovery from hurricane Katrina in the lower Pearl River flood plain of Louisiana, USA. *Wetlands*, *29*, 66–79.

Ramsey, E., III, Rangoonwala, A., Suzuoki, Y., & Jones, C. (2011). Oil detection in a coastal marsh with polarimetric SAR. *Remote Sensing*, *3*, 2630–2662.

Ramsey, E., III, Sapkota, S., Baarnes, F., & Nelson, G. (2002). Monitoring the recovery of marsh burns with the normalized difference vegetation index and Landsat Thematic Mapper data. *Wetlands Ecology and Management*, *10*(1), 85–96.

Ramsey, E., III, Suzuoki, Y., Rangoonwala, A., & Bannister, T. (2013). Coastal inundation monitoring with C-band and L-band satellite data. *JAWRA Journal of the American Water Resources Association*, *49*(6), 1239–1260.

Ramsey, E., III, Werle, D., Lu, Z., Rangoonwala, A., & Suzuoki, Y. (2009). A case of timely satellite image acquisitions in support of coastal emergency environmental response management. *Journal of Coastal Research*, *25*, 1168–1172.

Ramsey, E., III, Werle, D., Suzuoki, Y., Rangoonwala, A., & Lu, Z. (2012). Limitations and potential of optical and radar satellite imagery to monitor environmental response to coastal emergencies in Louisiana, USA. *Journal of Coastal Research*, *28*(2), 457–476.

Richter, R. (2010). *Atmospheric/topographic correction for satellite imagery (ATCOR-2/3 user guide, version 7.1)*. D-82234 Wessling, Germany: DLR-German Aerospace Center, 165 (DLR-IB 565-01/10).

Richter, R., & Schläpfer, D. (2011). Atmospheric/topographic correction for satellite imagery. *DLR report DLR-IB 565-02/11, Wessling, Germany* (pp. 202).

Sasser, C., Visser, J., Mouton, E., Linscombe, J., & Hartley, S. (2008). Vegetation types in coastal Louisiana in 2007. *U.S. Geological Survey open-file report 2008-1224* (URL: http://pubs.usgs.gov/of/2008/1224, accessed 20 October 2012).

Sasser, C., Visser, J., Mouton, E., Linscombe, J., & Hartley, S. (2014). *Vegetation types in coastal Louisiana in 2013: U.S. Geological Survey Scientific Investigations Map 3290.* (http://pubs.usgs.gov/sim/3290/, accessed 27 March 2014).

Strategic Online Natural Resources Information System (2009). *SONRIS integrated applications.* Baton Rouge, LA: Louisiana Department of Natural Resources (http://sonris-www.dnr.state.la.us/www_root/sonris_portal_1.htm, accessed 24 September 2013).

Van Zyl, J., & Ulaby, F. (1990). Scattering matrix representation for simple targets. In F. T. Ulaby, & C. Elachi (Eds.), *Radar polarimetry for geoscience applications* (pp. 17–52). Norwood, MA: Artech House, Inc.

Vogelmann, J., Rock, B., & Moss, D. (1993). *Red edge spectral measurements from sugar maple leaves14(8). (pp. 1563–1575), 1563–1575.*

Westman, W., & Paris, J. (1987). Detecting forest structure and biomass with C-band multipolarization radar: Physical model and field tests. *Remote Sensing of Environment*, *22*, 249–269.

Wickland, D. (1991). Mission to planet earth: The ecological perspective. *Ecology*, *72*, 1923–1933.

Zhang, M., Ustin, S., Reimankova, E., & Sanderson, E. (1997). Monitoring pacific coast salt marshes using remote sensing. *Ecological Applications*, *7*(3), 1039–1053.

Zheng, Y., Muellerschoen, R., Michel, T., Chapman, B., Hensley, S., & Lou, Y. (2010). Geocoding of UAVSAR data products. *IEEE Geoscience and Remote Sensing Symposium (IGARSS), 25–30 July, 2010, Honolulu, Hawaii.*